

Time Domain Modelling of Optical Add-drop filter based on Microcavity Ring Resonators

Nabeil A. Abujnah¹, Rosa Letizia², Fathi Alwafie³, Salah Obayya⁴

¹Department of Electrical and Electronic Engineering, Faculty of Engineering, University of Azzaytuna-Libya

²Engineering Department, Lancaster University, Lancaster, LA1 4YR.UK

³Department of Electrical and Electronic Engineering, Faculty of Science Engineering and Technology, University of Sebha-Libya.

⁴Centre for Photonics and Smart Materials, Zewail City of Science and Technology, Sheikh Zayed District, 6th of October city, Giza, Egypt

Abstract: In this paper an accurate analysis of two-dimensional (2D) coupled ring resonators based on high-index-contrast is carried out. The normalized transmission spectra for single-ring and double-ring configuration have been investigated by using a robust and accurate Multiresolution Time Domain (MRTD) technique with conjunction with uniaxial perfectly matched layer (UPML) absorbing boundary condition that rigorously terminate the computational window. The resonant-mode quality factors (Q), free spectral range (FSR) are numerically investigated. The variation of the structure parameters such as the symmetric and asymmetric gap size (g) lead to dramatic changes of Q and the extinction ratio of the device. Studies of the transmission characteristics for the ring diameter of $3.4 \mu\text{m}$ shows the possibility for achieving Q 's in several thousands and FSR of 9 THZ (80nm) in the $1.55 \mu\text{m}$ wavelength range.

Keywords:- multiresolution time domain, microcavity, numerical analysis ring resonators,, time domain methods.

I. Introduction

Recent advances in micro and nanofabrication technology have brought a new interest in building optical devices with physical dimension comparable to optical wavelength [1, 2]. In particular, microcavity resonators based on whispering-gallery-modes (WGMs) play significant role in many applications ranging from quantum electrodynamics to telecommunication devices and optical sensors [3-8]. At particular wavelength, light in the bus line waveguide can evanescently coupled through the gap into WGM of the resonator if proper phase matching conditions exist. By means of refractive index contrast between core and cladding, light which is travelling in medium of circular geometry such as rings can be resonantly confined by total internal reflection (TIR)[9]. These modes can resonate with high quality factor (Q) in the cavity where the long photons lifetimes allow the field within the cavity to be built from a considerably weaker input [10] [11]. Historically, the original concept of an optical ring resonator is back date to 1969[12], where relatively optical ring resonators made in direct laser written polymers[13], and ion-exchanged glass substrates[14], were demonstrated. However, due to low-index-contrast between the resonators medium and the surrounding material, the radius needed to be of the order of several centimetres to bend losses [1] [15]. In the last few years, research interest has been strongly directed to the design of optical ring resonators based on high-index-contrast semiconductor materials [1, 16, 17]. These research efforts have clearly demonstrated that these structures naturally permit realisation of small-radius microcavities with negligible bending losses resulting in large longitudinal mode spacing. For this reason, they enable the integration of a large number of devices on optical circuits foreseen for very large scale integrated (VLSI) photonics [1]. For active device applications, wide range of research studies can be found in literature on strongly guiding semiconductor ring laser with diameters ranging from 10 to 500 μm . and large waveguide width from 4 to 20 μm [18] [19] [20]. In order to acquire light output, these ring resonators are coupled to output by means of Y junction. Thanks to existing semiconductor fabrication techniques, light in the bus waveguide can be evanescently coupled through the gap into whispering gallery mode of the resonator if the proper phase matching conditions exist. Optical microring resonators (MRRs) based on high-index-contrast semiconductor waveguides are able to support strongly confined WGMs with diameters as small as 1-2 μm [1]. If the free spectral range (FSR) of the ring can be made wide enough to accommodate the set of WDM channels within the communication window, one can achieve the goal of dropping one channel by one filter without affecting the other channels. To ensure a FSR larger than the optical communication window (30nm), a ring radius of less than 5 μm is required. Since the MRRs have been recognised as complicated structures and cannot be analysed by using simple techniques, the characterisation of these devices usually necessitates a full-wave electromagnetic simulator. In order to choose a particular simulation approach, generally two criteria have to be taken into account. Firstly, the desired results needed to be accomplished with available resources and secondly,

CPU simulation time has to be optimised to obtain these results. Since the first aspect is related to the convergence rate of the used techniques, large computational problems can be studied with a highly convergent algorithm. On the other side, the execution simulation time not only relies on the cost of time per time step but also depends on the number of time steps that have to be carried out. Among the existing full-wave techniques, Finite Difference Time Domain (FDTD) is known as a popular framework for low-cost feasibility studies and permits design optimisation before fabricating the device[1]. Although this technique is straightforward and adaptable, it puts a heavy burden on computer resources specially when modelling complex problems with large computational volumes. The more sophisticated MRTD technique used here to analyse MRR devices [21-23]. This technique was introduced by Krumpolz and Katehi in 1996 [24] for the microwave range and has been recently extended also for the optical range [23]. This method uses a high order of approximation of derivative in space to reduce the numerical phase error of FDTD. By doing so, MRTD does not require the use of a very fine mesh size to discretise the structure geometry and high numerical accuracy can be achieved while mitigating the computational burden. Therefore, the possibility of saving CPU running time makes the MRTD an efficient alternative numerical scheme to the commonly used FDTD for the design of microring structures. In this paper, MRTD has been used to analyse the transmission characteristics of different order of MRR. The analysis is mainly focused on the extraction of different resonant mode where different investigation have been carried out to explore the effect of different parameters of the structure on transmitted and coupled power. Parameter such as gap size, the distance between two rings and the width of ring and waveguide have been varied and sets of different results have been presented. This paper is organized as following. Following this introduction, a brief mathematical analysis is given in section 2. The simulation results are presented in section 3. Finally conclusions are drawn.

II. Analysis

Starting from Maxwell's equation and for 2D structures in x-z plane, the transverse electrical mode (TE) with a components E_y , H_x and H_z is derived under assumption that y-axis is the homogeneous direction and the x-axis as the propagation direction.

$$\frac{\partial H_x}{\partial t} = \frac{1}{\mu_0} \frac{\partial E_y}{\partial z} \tag{1a}$$

$$\frac{\partial H_z}{\partial t} = -\frac{1}{\mu_0} \frac{\partial E_y}{\partial x} \tag{1b}$$

$$\frac{\partial E_y}{\partial t} = \frac{1}{\epsilon_0 \epsilon_r} \left(\frac{\partial H_x}{\partial z} - \frac{\partial H_z}{\partial x} \right) \tag{1c}$$

With respect to the unit cell shown in Fig. 1, the electromagnetic fields are expanded as combination of scaling function in space and Haar function in time using

$$E_y(x, z, t) = \sum_{n,i,j=-\infty}^{+\infty} E_{i+\frac{1}{2},j+\frac{1}{2}}^{y,\phi} \phi_{i+\frac{1}{2}}(x) \phi_{j+\frac{1}{2}}(z) h_{n+\frac{1}{2}}(t) \tag{2}$$

where n, i, and j are the discrete indexes in time and in space respectively, Φ is the scaling function representing the sampling in space, h is the Haar function, and $E_{i+\frac{1}{2},j+\frac{1}{2}}^{y,\phi}$ is the expansion coefficient for E_y component on which the iterative process of update is applied on.

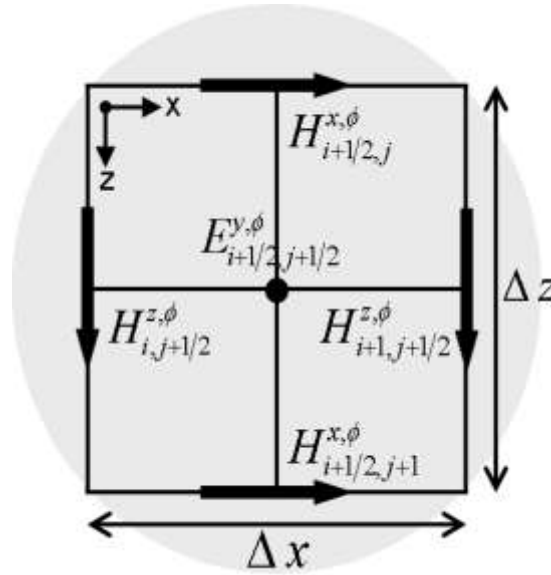


Figure 1: Electrical and magnetic field expansion as placed inside 2-D MRTD unit cell.

Substituting the field expansions in the form of (4) into the scalar Maxwell's equations and testing them with the dual of the biorthogonal scaling function $\tilde{\phi}_m$ (with $m = i, j$), by applying the method-of-moments, lead to the discretised update equations [23]:

$${}^{n+1}H_{i+\frac{1}{2},j}^{x,\phi} = {}^nH_{i+\frac{1}{2},j}^{x,\phi} - \frac{\Delta t}{\mu_0 \Delta z} \times \left(\sum_{l=-L_s}^{L_s-1} a(l) {}^{n+\frac{1}{2}}E_{i+\frac{1}{2},j-l-\frac{1}{2}}^{y,\phi} \right) \quad (3a)$$

$${}^{n+1}H_{i,j+\frac{1}{2}}^{z,\phi} = {}^nH_{i,j+\frac{1}{2}}^{z,\phi} + \frac{\Delta t}{\mu_0 \Delta x} \times \left(\sum_{l=-L_s}^{L_s-1} a(l) {}^{n+\frac{1}{2}}E_{i-l-\frac{1}{2},j+\frac{1}{2}}^{y,\phi} \right) \quad (3b)$$

$${}^{n+\frac{1}{2}}E_{i+\frac{1}{2},j+\frac{1}{2}}^{y,\phi} = {}^{n-\frac{1}{2}}E_{i+\frac{1}{2},j+\frac{1}{2}}^{y,\phi} + \frac{\Delta t}{\epsilon_0 \epsilon} \times \left(\sum_{l=-L_s}^{L_s-1} a(l) \times \left(-\frac{1}{\Delta z} {}^nH_{i+\frac{1}{2},j+\frac{1}{2}}^{x,\phi} + \frac{1}{\Delta x} {}^nH_{i-l-1,j+\frac{1}{2}}^{z,\phi} \right) \right) \quad (3c)$$

where μ_0, ϵ_0 are permeability and permittivity of the free space respectively, ϵ is the relative permittivity of the medium, and Δt is time step. Δx and Δz are the spatial increments in the direction of x and y respectively. The 'stencil size' L_s stand for the effective support of the basis function that determines the number of expansion coefficients considered in the summation and it is equal to 5 for CDF(2,4), while $a(l)$ represent the connection coefficients that can be numerically calculated using [23]

$$\int_{-\infty}^{+\infty} \phi_l(x) \frac{\partial \phi_{i+\frac{1}{2}}(x)}{\partial x} dx = \sum_{l=-L_s}^{L_s-1} a(l) \delta_{i+l,i} \quad (4)$$

The values of the connection coefficients $a(l)$ for the case of CDF(2,4) are reported in [22].

In order to ensure the numerical stability of the MRTD scheme, the time interval Δt has to be smaller than a certain limit, as follows

$$\Delta t \leq s \frac{\Delta}{c_0} \quad (5)$$

with

$$s = \frac{1}{\sqrt{2} \sum_{l=0}^{L_s-1} |a(l)|} \quad (6)$$

where $\Delta = \Delta x = \Delta z$, c_0 is the speed of the light, and the Courant number s represents the stability factor which is conveniently fixed to 0.1 through the paper [23].

The uniaxial perfectly matched layers (UPML) are a very efficient and robust way to terminate the computational domain with layers of artificial absorbers that capable of very-low reflection and it has been successfully incorporated with MRTD scheme as boundary conditions. As an example, the discretised equations to update E_y component through the displacement vector D_y are reported here

$$\begin{aligned}
 {}^{n+\frac{1}{2}}D_{i+\frac{1}{2},j+\frac{1}{2}}^{y,\phi} &= \left(\frac{2\varepsilon_0 - \sigma_z \Delta t}{2\varepsilon_0 + \sigma_z \Delta t} \right)^n {}^n D_{i+\frac{1}{2},j+\frac{1}{2}}^{y,\phi} \\
 &+ \left(\frac{2\varepsilon_0 \Delta t}{2\varepsilon_0 + \sigma_z \Delta t} \right) \sum_{l=-L_s}^{L_s-1} a(l) \left(-\frac{{}^n H_{i+\frac{1}{2},j-l-1}^{x,\phi}}{\Delta z} + \frac{{}^n H_{i-l-1,j+\frac{1}{2}}^{z,\phi}}{\Delta x} \right) \quad (7a)
 \end{aligned}$$

$$\begin{aligned}
 {}^{n+\frac{1}{2}}E_{i+\frac{1}{2},j+\frac{1}{2}}^{y,\phi} &= \left(\frac{2\varepsilon_0 - \sigma_x \Delta t}{2\varepsilon_0 + \sigma_x \Delta t} \right)^n {}^n E_{i+\frac{1}{2},j+\frac{1}{2}}^{y,\phi} \\
 &+ \left(\frac{2\varepsilon_0}{\varepsilon_0 \varepsilon_{i+\frac{1}{2},j+\frac{1}{2}} (2\varepsilon_0 + \sigma_x \Delta t)} \right) \times \left({}^{n+\frac{1}{2}}D_{i+\frac{1}{2},j+\frac{1}{2}}^{y,\phi} - {}^{n-\frac{1}{2}}D_{i+\frac{1}{2},j+\frac{1}{2}}^{y,\phi} \right) \quad (7b)
 \end{aligned}$$

where ε is the relative permittivity of the medium, and σ_x and σ_z are the electric conductivities of the UPML along x and z direction, respectively. Analogue equations are derived for the magnetic field components [23].

For the best performance of UPML absorbing boundary conditions, the parameter, σ_i ($i=x, z$) is chosen to vary in space as

$$\sigma_i(i) = \frac{\sigma_{\max} i^m}{d^m} \quad (8)$$

where $i=x, z$, d is the depth of the UPML, and m stands for the order of the polynomial variation. The choice of σ_{\max} that minimises reflection from the boundaries is [25]

$$\sigma_{\max} \cong \frac{(m+1)}{150\pi\Delta\sqrt{\varepsilon_r}} \quad (9)$$

where Δ is the spatial discretisation adopted, $i=x, z$, d is the depth of the UPML, and m stands for the order of the polynomial variation. The choice of σ_{\max} that minimises reflection from the boundaries is [25]

$$\sigma_{\max} \cong \frac{(m+1)}{150\pi\Delta\sqrt{\varepsilon_r}} \quad (9)$$

where Δ is the spatial discretisation adopted.

III. Results And Discussion

As a first structure, the single MRR shown in Fig. 2 has been considered where the width $W = 0.3 \mu\text{m}$, the ring diameter $d = 3.4 \mu\text{m}$, and the core and the cladding have refractive indices of $n_{\text{core}} = 3.2$ and $n_{\text{cl}} = 1$ respectively.

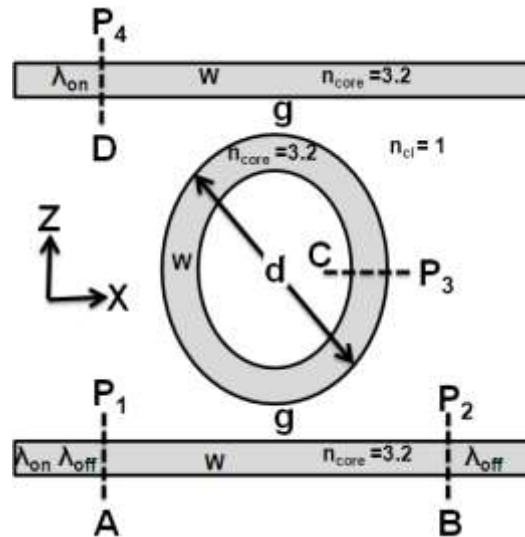


Figure 2: Schematic of microring resonator coupled to two straight waveguides.

The structure is discretised into a uniform mesh with cell size $\Delta_x = \Delta_z = \Delta = 27.25$ nm and is terminated by 20-cell UPML to absorb the reflected power. It is important to notice that the chosen Δ is about twice the value required by previous analysis of MRR structures by means of FDTD as found in [1]. Where the same level of accuracy can be achieved and the possibility to save the CPU running time also can be obtained. A Gaussian shaped pulse in space with central frequency $f = 200$ THz ($\lambda = 1.5\mu\text{m}$), modelled with Gaussian pulse in time, has been used to excite the structure to cover the frequency range of interest. As shown in Fig. 2, different cross-sections are chosen in order to record the time domain variation the incident, transmitted, and reflected fields. By means of Fast Fourier Transform (FFT) of the recorded time-dependent fields, the coupled power at port C and the transmitted power at port B are calculated by dividing the coupled and transmitted spectra by incident spectrum at port A, respectively. The effect of the gap size, g on coupled power, κ and Q is shown in Fig.3 at the resonance mode of 1503 nm.

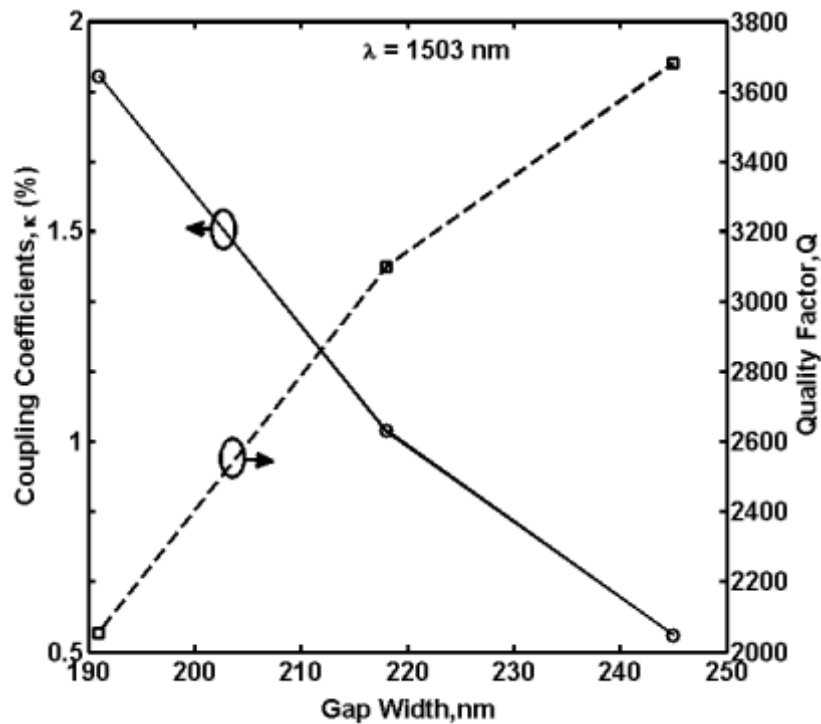


Figure 3: Effects of the gap width on the resonance quality factor and coupling coefficients.

It is apparent that increase of g has significant effect on both Q and κ . Since with the increase in gap size, the coupling efficiency of the resonance modes decreases due to a small fraction of power exchanged, while the Q value increases. The coupling efficiency can be enhanced in order to compensate the losses in the cavity and this will improve the transmission. However, the quality factor will be degraded. For this reason, the optimum values of gap size need to be carefully chosen in order to achieve reasonable high quality factor, while the coupling efficiency is within desirable range. According to Fig. 3, a good compromise can be achieved by choosing the $g = 218$ nm where the values of the κ and Q are 1.024 % and 3098 respectively. Next, the transmission at port B for 3.4 μm -diameter ring and 218 nm of g is considered.

The measured transmission spectrum of single-ring resonator around $\lambda = 1.55$ μm is presented in Fig. 4.

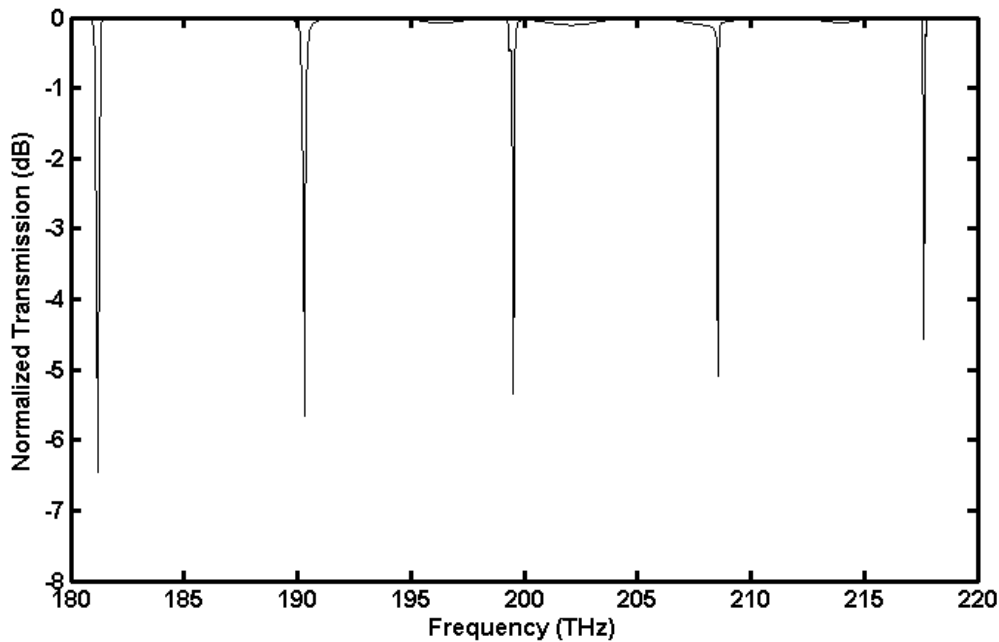


Figure 4: MRTD-computed Transmission for 1.7- μm -radius microring resonator coupled to straight 0.3- μm -wide waveguides.

From this figure, the localised resonance wavelength and Q 's and corresponding coupling efficiency are listed in table I.

TABLE I Resonance Data from Fig.4 for 3.4 μm -Diameter MRR and $w = 0.3$ μm

| m | F (THz) | λ_{res} (nm) | Q |
|-----|---------|-----------------------------|------|
| 18 | 181.2 | 1655.62 | 1295 |
| 19 | 190.3 | 1576.45 | 1455 |
| 20 | 199.4 | 1504.51 | 3098 |
| 21 | 208.5 | 1438.84 | 2937 |
| 22 | 217.6 | 1378.67 | 3680 |

The Q 's of the m^{th} resonance is extracted directly from power spectrum by forming the ratio of the resonant wavelength (λ_m) to the width of the resonance ($\delta\lambda$) at the half-power points. The FSR which defined as the spacing between two adjacent resonant wavelengths ranges between 60 to 80 nm. The rejection ratio or on/off ratio which is the ratio of power transmitted at resonance wavelength to the power not transmitted at resonance wavelength is approximately 6dB. Fig.5 shows the variation of extinction ration as a function of gap size.

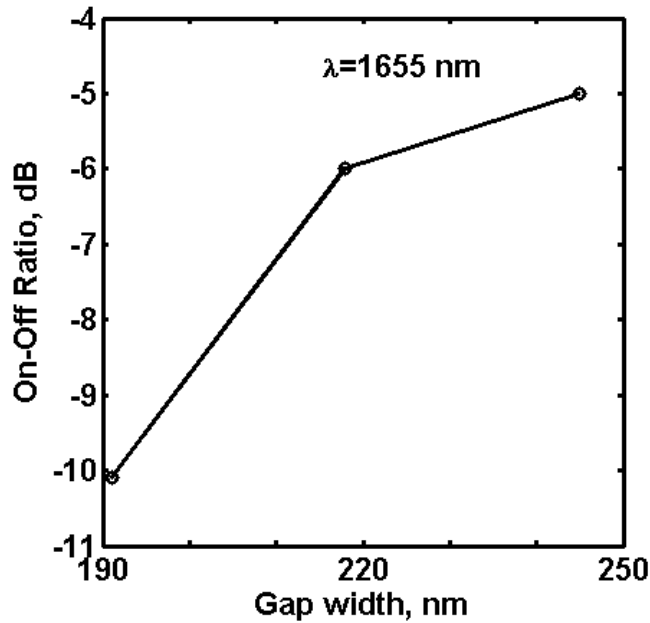


Figure 5: Effects of the gap width on the on-off ratio.

As can be seen from Fig. 5, the extinction ratio can be altered by varying the coupling efficiency, κ . However, the Q will be also affected in this manner as indicated from Fig. 3. Even though the rejection ratio required being large enough to minimize the crosstalk, the quality factor needed to be high in some application related to WDM. In order to increase the extinction ratio while the reasonable quality factor can be also obtained, double parallel microcavity ring resonators (DPMRR) is suggested. The structure, shown in Fig. 6 consists of two parallel ring resonators centred between two straight waveguides.

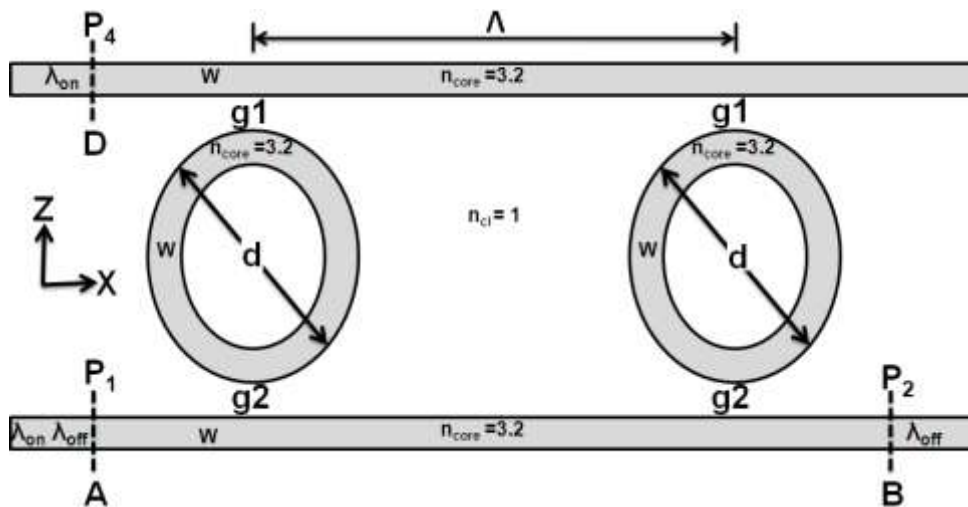


Figure.6: parallel coupled microring resonators, double ring case.

The following selections of parameters are chosen as following: the diameters of all rings are $d = 3.4 \mu\text{m}$, the core and the cladding have refractive indices of $n_{\text{core}} = 3.2$ and $n_{\text{cl}} = 1$ respectively, the widths of all rings and straight waveguides are $W = 0.3 \mu\text{m}$, the gap width between the outer rings and straight waveguides is set to be 218 nm. The structure is excited in the same manner as in single ring. The distance from centre to centre denoted by Λ between two rings is set to $5 \mu\text{m}$. The transmission characteristic shown in Fig. 7 is achieved using DPMRR.

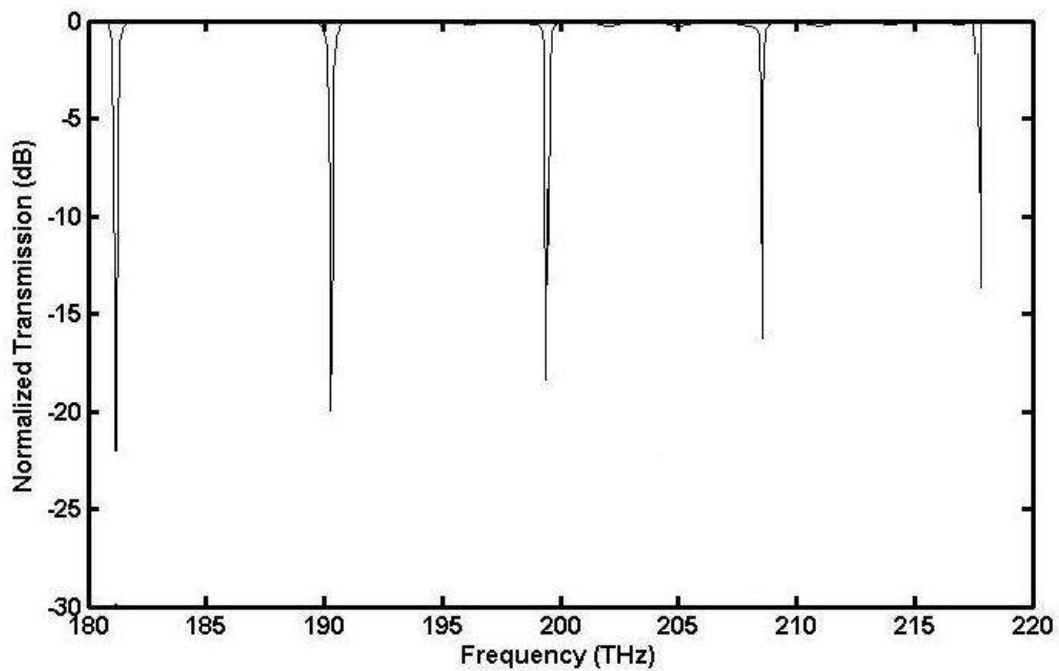


Figure.7: MRTD-computed Transmission for 1.7- μm -radius double microring resonator coupled to straight 0.3- μm -wide waveguides where the distance between two rings is 5 μm .

The localised resonance wavelength is extracted and Q's of the m^{th} resonance is calculated directly from power spectrum in the same manner as in single ring case. These results are listed in table II.

Table II Resnace Data From Fig. 7 For 3.4- μm -Diameter PDMRR and $w = 0.3 \mu\text{m}$

| m | F (THz) | λ_{res} (nm) | Q |
|----|---------|-----------------------------|------|
| 18 | 181.2 | 1655.62 | 1242 |
| 19 | 190.3 | 1576.45 | 1312 |
| 20 | 199.4 | 1504.51 | 2819 |
| 21 | 208.5 | 1438.84 | 3284 |
| 22 | 217.6 | 1378.67 | 3666 |

As shown in this table, there is slightly change in the quality factor. While the on- off ratio ranges between 4 to 11 dB at different resonance wavelengths. The effect of changes in the gap size between the input and output waveguides and the ring is considered. Two types of changes of g_1 and g_2 are discussed. Change both gap identically, and change only one of the gap size while keeping the other constant. Figure 8 and 9 show the effect of the symmetrical change where $g_1 = g_2 = 191 \text{ nm}$ and asymmetrical change where $g_1 = 191 \text{ nm}$ and $g_2 = 245 \text{ nm}$. The distance between two rings set to $\Lambda = 5 \mu\text{m}$. Based on the coupling which decreases at high frequencies, the Q should increase with frequency. Such behaviour is observed in Fig. 8.

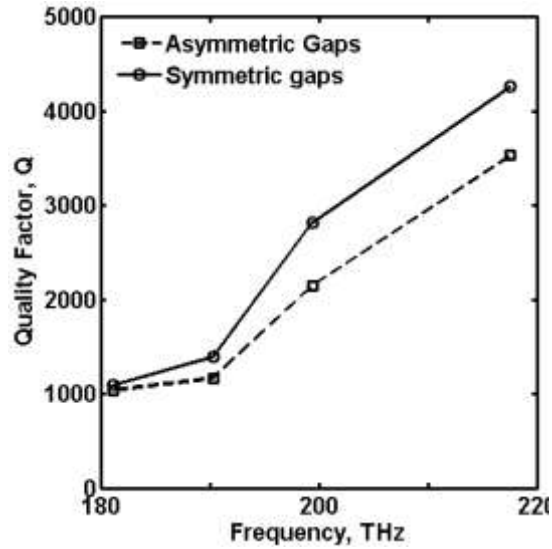


Figure.8: Effects of symmetrical and asymmetrical change of both separation distances on the quality factor.

However, as the gap width g_1 , g_2 are reduced, the coupling efficiency between the straight input waveguide and the cavity increases while the transmitted power at throughout port decreases. Due to the decrease in the level of transmitted power at throughout port higher on-off ratio is achieved while the level of the Q is decreased. Figure 9 shows the MRTD results for DPMRR for asymmetric gap width.

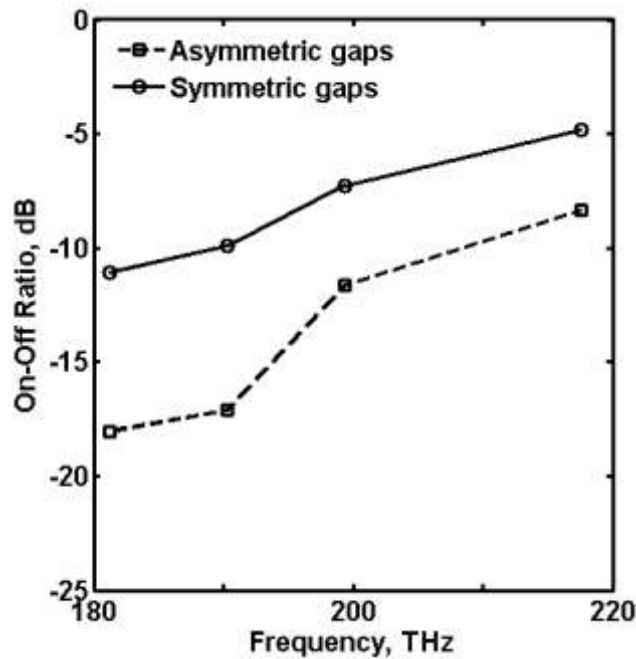


Figure. 9: Effects of symmetrical and asymmetrical change of both separation distances on the on-off ratio.

Keeping the gap width g_1 constant and g_2 is increased, and then the coupling between the input waveguide and the cavity increases. Due to the increase the level of coupling power, the level of transmitted power at throughout port decreases. On the other hand, keeping the gap width g_1 constant, if g_2 is increased, then the coupling between the output waveguide and the cavity decreases. As more power is remained in the cavity, the Q is increased while the level of on-off ratio decreases. Figure 10 shows the electric field pattern between the waveguide and the cavity when a sinusoidal continues wave has been injected and reached the steady state. The wavelength of the sinusoidal is fixed at 1655 nm (181.2 THz). As shown in this figure, nearly 100 % of the power is switched to the cavity which in turn switched to the output waveguide.

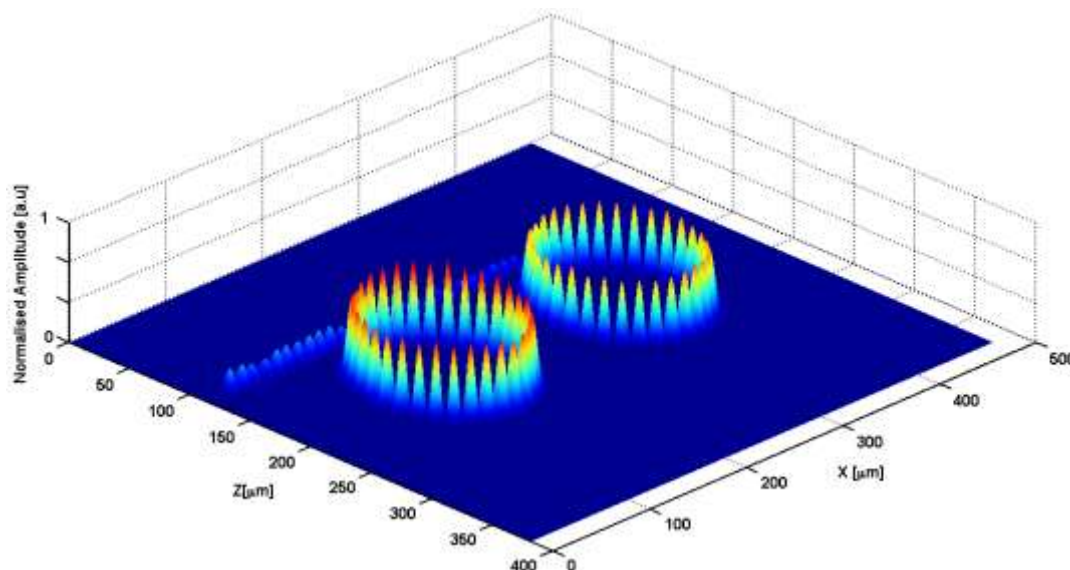


Figure.10: Sinusoidal steady-state amplitude distributed in 1.7- μm -radius microring resonator: ON-resonance at 1655 nm

In the same manner, the steady-state E-field is computed for excitation at nonresonant wavelength 1615 nm (185.7 THz) is illustrated in Fig 11. As shown in this figure, no coupling occurred between the input waveguide and the cavity and 100 % of the signal is transmitted at output at port B.

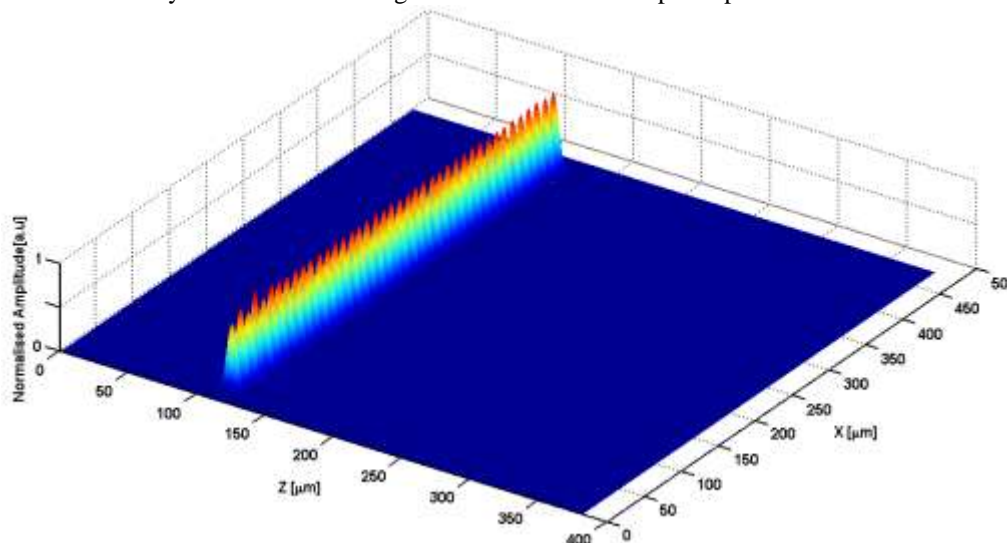


Figure.11: Sinusoidal steady-state amplitude distributed in 1.7- μm -radius microring resonator: OFF-resonance at 1615 nm

IV. Conclusion

In this paper, optical microcavity ring resonator based on high-index-contrast waveguide have been analysed by using MRTD formulation based on CDF (2, 4) scaling function and rigorous UPML boundary conditions. The approach has proved good level of accuracy in extracting and studying the resonance behaviour of this structure. The optimisation of a number of important parameters, including coupling coefficients, quality factor, and rejection ratio has been discussed. A high-order structure consisting of a two ring resonators in parallel with centre distance of 10 μm has shown interesting potential in increasing the on-off ratio where it is desirable to minimise the cross talk of the device. Furthermore, by using asymmetric gap sizes, the rejection ratio of the device has significantly increased of about 60 %, compared to the best result as in the symmetric gap size case.

References

- [1]. Taflove A., Hagness S. C.: 'Computational electrodynamics: The finite-Difference Time-Domain Method' (Artech House, Norwood, Inc, 2005)
- [2]. Slusher R. E.: 'Optical processes in microcavities', *semicond. Sci. Technol.*, 1994, 9, (11S), pp. 2025-2030
- [3]. Guarino A., Poberaj G., REZZONICO D., DEGL'INNOCENTI R., GUNTER P.: 'Electro-Optically tunable microring resonators in lithium niobate', *Nature Photonics*, 2007, 1, pp. 407–410
- [4]. Vahala K. J.: 'Optical microcavities', *Nature*, 2003, 424, (6950), pp. 839-846
- [5]. Grove R., Van V., Ibrahim T. A., Absil P. P., Calhoun L. C., Johnson F. G., Hryniewicz J. V., Ho P. T.: 'Parallel Cascaded semiconductor microring resonators in high order and wide-FSR filters', *J. Lightwave Technol.*, 2002,20,(5), pp. 900-905
- [6]. Rabus D. G., Hamacher M., Troppenz U., Heidrich H.: 'High-Q channel-dropping filters using ring resonators with integrated SOAs', *IEEE Photon.Technol. Lett.*, 2002,14,(10), pp. 1442-1444
- [7]. Simos H., Hesaritakis C., Alexandropoulos D., Syyridis D.: 'Intraband crosstalk properties of add-drop filters based on active microring resonators', *IEEE Photon.Technol. Lett.*, 2007,19,(17/20) pp. 1649-1651
- [8]. Chao C. Y., Fung W., Guol. J.: 'Polymer microring resonators for biomedical sensing applications', *IEEE J .Sel. Top. Quantum Electron.*, 2006,12,(1), pp. 134-142
- [9]. Arnold S.: 'Microsheres photonic atoms and the physics of nothing', *American Scientist*, 2001, 89,(5), pp. 414-421
- [10]. Blair S., Chen Y.: 'Resonance-enhanced evanescent-wave fluorescence biosensing with cylindrical optical cavities', *Applied Optics*, 2001,40,(4), pp. 570-582
- [11]. Rayleigh L.: 'The Problem of the Whispering Gallery', in *Scientific Papers*, Cambridge University, Cambridge, England, 1912, 5, pp. 617–620, 1912.
- [12]. Marcattilio. A. J.: 'Bends in Optica Dielectric Guides', *J.The Bell System Technol.*, 1969, 48,(7), pp. 2103-2132
- [13]. Haavisto J., Pajar G. A.: 'Resonance effects in low-loss ring waveguides', *Opt. Lett.*, 12,(5), pp. 510—512
- [14]. Honda K., Garmire E. M., Wilson K. E.: 'Characteristics of an integrated optics ring resonator fabricated in glass', *J. Lightwave Technol*, 1984, 5, (2), pp. 714-719
- [15]. Smith. K., Pennings E. C. M., Blok H. B.: 'A normalized approach to the design of low-loss optical waveguide bends', *J. Lightwave Technol*, 1993, 11,(11), pp. 1737—1742
- [16]. Rafizadeh D., Zhang J. P., Hagness S. C., Taflove A., Stair K. A., Ho S. T.: 'Waveguide-coupled AlGaAs/GaAs microcavity ring and disk resonators with high finesse and 21.6-nm free spectral range', *Opt. Lett.*, 1997, 22,(16), pp. 1244-1246
- [17]. Barwicz T., Popovic M., Watts M. R., Rahich P. T., Ippen E. P., Smith H. I.: 'Fabrication of add-drop filter based on frequency-matched microring resonators', *J. Lightwave Technol*, 2006,24,(5), pp. 2207-2218
- [18]. Jezierski A. F., Laybourn P. J. R.: 'Integrated semiconductor ring lasers', *Inst. Elect. Eng. Proc. J*, 1988, 135, (1) pp. 17-24
- [19]. Kruss T., Laybourn P. J. R., Roberts J.: 'CW operation of semiconductor ring lasers', *Electron. Lett.*, 1990, 26, (25), pp. 2095-2097
- [20]. Hohimer J. P., Carft D. C., Hadley G. R., Vawter G. A., Warren M. E.: 'Single-frequency continuous-wave operation of ring resonator diode lasers', *App. Phys. Lett.*, 1991,59,(23), pp. 3360-3362
- [21]. Tentzeris E. M., Robertson R. L., Harvey J., Katehi L.: 'Stability and dispersion analysis of Battle-Lemarie based MRTD scheme', *IEEE Tran.Microwave theory Tech.*, 1999,47,(7), pp. 1004-1013
- [22]. Dogaru T., Carin L.: 'Multiresolution Time-Domain Using CDF Biorthogonal wavelet', *IEEE Tran.Microwave theory Tech.*, 2001, 49,(5), pp. 685-691, 2001.
- [23]. Letizia R., Obayya S. S. A.: 'Efficient multiresolution time domain analysis of arbitrary shaped photonic devices', *IEEToptoelectronics*, 2008,2,(6), pp. 241-253
- [24]. Krumpholz M., Katehi L. P. B.: 'MRTD: new time domain scheme based on multiresolution analysis', *IEEE Tran.Microwave theory Tech.*, 1996,44,(4), pp. 555-571
- [25]. Zhu X., Dogaru T., Carin L.: 'Three-Dimensional Biorthogonal Multiresolution Time-Domain Method and Its application to Electromagnetic Scattering Problems', *IEEE Tran.On Antennas and Propag.*, 2003,51,(5) pp. 1085-1092.